AIAA JOURNAL
Vol. 36, No. 10, October 1998

Prediction Method of Unsteady Combustion Around Hypersonic Projectile in Stoichiometric Hydrogen–Air

Akiko Matsuo*
Keio University, Yokohama 223-8522, Japan
and
Kozo Fujii†
Institute of Space and Astronautical Science, Sagamihara 229-8510, Japan

An effective nondimensional parameter, referred to as the first Damköhler parameter, is proposed to quantitatively classify the unsteady flow regime of shock-induced combustion around a hypervelocity spherical projectile in the stoichiometric hydrogen–air mixture. The parameter consists of the ratio of the fluid characteristic timescale to the chemical characteristic timescale. The fluid characteristic time is defined as a projectile diameter divided by a speed of sound behind the normal segment of the steady bow shock. The chemical characteristic time is defined as a temperature behind the normal segment of the steady bow shock over the maximum temperature increase per unit time for the exothermicity. The temperature increase for the exothermicity is estimated by the time integration of the species equations in the zero dimension in space. The proposed first Damköhler number can be analytically computed by the chemical and fluid characteristics only, without ballistic range experiments or expensive simulations on high-performance computers. The parameter is quantitatively characterized from the two distinct flow regimes observed in the experimental and numerical results. Also, features of the transition between two regimes are clarified by changing the projectile diameter, the projectile speed, and the test gas pressure.

Introduction

INSTABILITIES of shock-induced combustion around hypersonic spherical projectiles into quiescent detonable gases were observed in a number of ballistic range experiments[1–6] in the 1960s and 1970s. The experimental photographs with spark light sources revealed the presence of widespread density variation spaced in a remarkably periodic manner over the whole region within the bow shock of the projectiles. These periodic density variations appear in two distinct regimes[1]: One is referred to as the regular regime, whose density variations are highly regular and low in amplitude (high-frequency mode), and the other is referred to as the large-disturbance regime, whose oscillations are less regular and low in frequency but far more pronounced (low-frequency mode). A period of the oscillation is normalized by the induction time t_{ind} in the nearly uniform region behind the normal segment of the bow shock, and the period of the large-disturbance regime is several times longer than that of the regular regime. The period in both the regular and the large-disturbance regimes depends on the projectile speed and is also a function of the induction time derived from the projectile velocity. The experimental results[1] suggested that the range of the period of the large-disturbance regime is $3 < t/t_{\text{ind}} < 12$, and the averaged period of the large-disturbance regime derived by the method of least squares was 5.23. On the other hand, the period of the regular regime oscillations is about 1.15. Both the regular and large-disturbance regimes are unsteady flowfields with respect to the projectile as the density variations are intermittently created in front of the projectile. Both regimes have been observed in hydrogen–oxygen-diluent, as well as hydrocarbon–oxygen-diluent, mixtures.

The mechanism of both the regular and the large-disturbance regimes have been numerically clarified by recent investigations.[7–16] In the work of Matsuo and Fujiwara[7] and Matsuo et al.,[8] a wave-interaction model on the stagnation streamline was proposed for the regular regime based on the simulation results. The frequencies in the simulation results quantitatively agreed with Lehr's experiments.[3] The simulation results of the other researchers supported the validity of the proposed model,[9–13] and the mechanism also was essentially the same as McVey and Toong's mechanism.[4] In the work of Matsuo and Fujii,[14,15] the mechanism of the large-disturbance regime is clarified by a series of simulations, and the wave-interaction model on the stagnation streamline was proposed, which was different from the model previously proposed by Alpert and Toong[1] in 1972. This proposed model was also supported by computational work by Ahuja and Tiwari.[16]

The recent simulation technique allows us to quantitatively discuss the detailed physics of the coupling between gas dynamics and chemical kinetics, and a number of simulation results have clarified the mechanism. However, a criterion for the prediction of the unsteady shock-induced combustion around the spherical projectile has not yet been established. In the present paper, the prediction method of the unsteady combustion regime of shock-induced combustion is newly proposed and is validated by the experimental and computational results.

Previous Studies

There has been an effort to explain the instabilities around the projectiles by using one-dimensional theoretical analysis of piston-supported detonations. Abouseif and Toong[17] analyzed the stability of the one-dimensional piston-supported gaseous detonations and found the low- and high-frequency modes previously reported in the numerical simulations of Fickett and Wood.[18] Both oscillation periods and amplification rates obtained by the exact linearized stability analysis[17] agreed well with those of the numerical calculations by Fickett and Wood. The predicted periods also agreed well with those observed in the blunt-body flow experiments.[1] But the analysis was still insufficient for the prediction of the onset of the unsteady flow regime, such as a regular or large-disturbance regime, under an arbitrary condition.

Alpert and Toong[1] showed that a necessary condition for the existence of the wave-interaction cycle of the large-disturbance regime is that the value of the second Damköhler parameter (the dimensionless specific enthalpy of reaction) be above a threshold value of approximately 0.5. The second Damköhler parameter is defined as $Q_n = Q/C_pT_0$, where Q_n is the net heat release per unit mass of gas mixture and T_0 is the gas temperature immediately behind the

Presented as Paper 96-3137 at the AIAA/ASME/SAE/ASEE 32nd Joint Propulsion Conference, Lake Buena Vista, FL, July 1–3, 1996; received Jan. 18, 1997; revision received Feb. 10, 1998; accepted for publication May 24, 1998.

*Assistant Professor, Department of Mechanical Engineering. E-mail: matsuo@mech.keio.ac.jp. Member AIAA.
†Professor, High-Speed Aerodynamic Division. Associate Fellow AIAA.

normal segment of the bow shock. Their specified condition was supported by their experiments.[1] However, this condition was not a sufficient condition for the onset of the large-disturbance regime, as both steady flow and regular regimes were also observed even when the second Damköhler number exceeded 0.5. They conjectured that the long-period wave-interaction cycle definitely requires a large change in bow shock strength for the initiation. The entry of the projectile into a reactive mixture through a diaphragm could provide the triggering perturbation. When the perturbation is not sufficiently strong, the regular or steady-flow regimes can result. Therefore, an initial disturbance of rather high intensity is needed to trigger the interactions for the large-disturbance regime. The second Damköhler parameter was used to identify the flow regime in the described analysis. The total heat release by the exothermicity was used as a key factor for the unsteady flow regime, regardless of the process of the heat release. Alpert and Toong[1] themselves described how the second Damköhler parameter is imperfect to quantitatively predict the unsteady flow regime of shock-induced combustion.

Development of a New Prediction Method

A series of computations[14] were carried out by changing the intensity of the concentration of the heat release at the reaction front on the stagnation streamline. The simulation results have revealed the importance of the process of the heat release. The strength of waves created at the new reaction region is extremely dependent on the process of the heat release as the chemical characteristic. However, the idea was not sufficient for the quantitative prediction of the unsteady regime under arbitrary conditions. What we need is a prediction method that can tell us which regime will occur when parameters such as a projectile diameter, a projectile velocity, and a gas mixture are given.

As for the strength of the unsteadiness, Ruegg and Dorsey[2] suggested that the test gas pressure is one of the important parameters to identify the unsteady flow regime. The numerical study by Ahuja and Tiwari[16] showed the dependence on the projectile diameter and the test gas pressure and clarified that the projectile length scale may change the flow regime, even when the test gas conditions are kept the same. Therefore, the projectile length scale is considered to be one of the important factors for the strength of the unsteadiness.

In general, two kinds of reference scales exist in chemical reacting flow problems; one is a fluid dynamics scale, and the other is a chemical kinetics scale. Normally, the gas pressure is regarded as a reference length scale of chemical kinetics, and the projectile diameter is regarded as a reference length scale of the fluid dynamics. The relation of these two reference scales must be important for the present flow phenomenon. Thus, the method of prediction should be determined considering the relation of the two kinds of reference scale problems. For that purpose, we first derive the parameters from the flowfield, and two parameters are set up based on the test gas condition and the projectile scale. One parameter represents the chemical kinetics part, and the other parameter represents the fluid dynamics part. Eventually, a nondimensional parameter, such as first Damköhler number, is utilized for the prediction of the unsteady shock-induced combustion as a single parameter using these two characteristics values. The first Damköhler number consists of the ratio of the fluid characteristic timescale to the chemical characteristic timescale. However, the characteristic values are not uniquely determined from the test gas conditions. Therefore, effective values representing the chemical and the fluid characteristics should be proposed to identify the unsteady regime and will be investigated in the following. First, the fluid characteristic timescale is considered. There are choices for the length scale of the fluid dynamics for blunt-body problems with chemical reactions. Considering the mechanism of the unsteady flow regime proposed as the wave-interaction model on the stagnation streamline in previous works,[7,8,14,15] the shock standoff distance on the stagnation streamline may be taken as a representative length scale. Because the Mach number range considered here is restricted to be between 4 and 6, the shock standoff distance simply depends on the blunt-body diameter. Therefore, the fluid characteristics length scale is represented by the projectile diameter. Next, the reference speed is required to define the characteristic timescale. At the reaction front, compression waves or reaction shock waves are generated, and these waves propagate behind the bow shock of the projectile. The wave propagation speed can be estimated using the speed of sound immediately behind the bow shock. Therefore, the speed of sound behind the bow shock is taken as a reference speed. Based on the length scale and the speed just defined, the characteristics timescale for the fluid part is defined as

$$t_f = D/a_2 \tag{1}$$

where D and a_2 indicate the projectile diameter and the speed of sound, respectively. The subscript 2 indicates the condition immediately behind the normal segment of the bow shock in front of the spherical projectile. It can be easily obtained by the normal shock relations under the real gas effects without flow simulations.

Next the chemical characteristic timescale is proposed as follows: Here, the intensity of the heat release that represents the chemical characteristics is quantitatively defined. The temperature-increasing profile for the exothermicity, which is obtained by time integration of the species equations in zero dimension in space under the constant volume mode, is used to represent the chemical characteristics. The zero-dimensional procedure gives us the time-evolving temperature profile. In the authors' previous works,[14] it has been clarified that the strength of the waves released from the reaction front significantly affects an onset of the unsteadiness. When the stronger wave (reaction shock) is released at the reaction front, the reaction shock could become a detonation wave, and the large-disturbance oscillation is established. When the weaker wave (compression wave) is released, the flow goes into the regular regime. Supposing that the speed of sound and the total heat release for the exothermicity are constant, the strength of the wave front can be determined by the maximum value of the temperature increase per unit time $(\mathrm{d}T/\mathrm{d}t)_{\max}$ (Fig. 1). Because the reaction occurs behind the bow shock, the temperature T_2 is used for the normalization. This idea does not require the total amount of the heat release. The chemical characteristics timescale is now defined as

$$t_c = T_2 \Big/ \left(\frac{\mathrm{d}T}{\mathrm{d}t}\right)_{\max} \tag{2}$$

Finally a nondimensional parameter (the first Damköhler parameter D_I) is defined and is proposed for the prediction. The definition is as follows:

$$D_I = \frac{t_f}{t_c} = \left(\frac{D}{a_2}\right) \Big/ \left[T_2 \Big/ \left(\frac{\mathrm{d}T}{\mathrm{d}t}\right)_{\max}\right] = D\left(\frac{\mathrm{d}T}{\mathrm{d}t}\right)_{\max} \Big/ (a_2 T_2) \tag{3}$$

Note again that the timescale for the fluid part can be computed without the flow simulation. The speed of sound a_2 is given immediately behind the normal segment of the bow shock by the normal shock relations under the real gas effects, and the projectile diameter D is in the test conditions. The scale for the chemical part can be computed based on the zero-dimensional analysis by time integration of the species equations in zero dimension in space and the normal shock relations under the real gas effects.

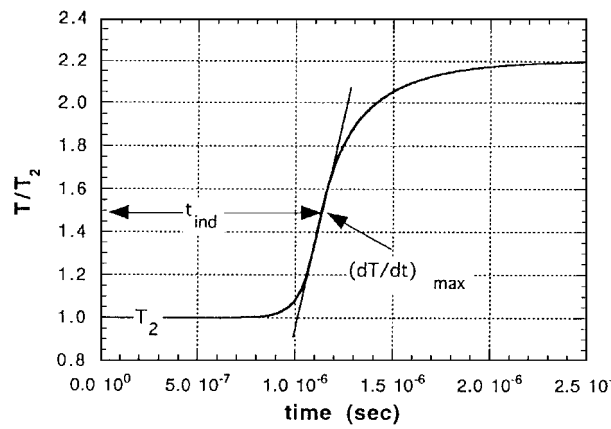

Fig. 1 Temperature profile by the time integration of the species equations under the constant volume and energy mode.

Computational Setup

To validate the prediction method, a series of computations were carried out. The governing equations are Euler equations under the axisymmetric assumption, and the chemical reaction is considered as a hydrogen–oxygen mechanism consisting of 8 species and 19 elementary reactions, omitting nitrogen reactions. The reproduction of the physical unsteadiness of all of the cases in Table 1 by our computational code has been confirmed by the previous computational works,[7,8,14,15] and the detailed computational setup was described in those papers.

The computational domain is limited to the region in front of the hemispherical body, and the flow is assumed to be axisymmetric based on the experimental observations. The number of grid points is 401×401, which are equally distributed in each direction. The grid refinement study in our previous work confirmed that this grid distribution is fine enough to reproduce the physical unsteady mode of shock-induced combustion.[16]

To capture physical instabilities derived by shock-induced combustion, initial disturbances introduced by the impulsive start of the computation should be avoided. Therefore, the following technique is used: The flowfield of the inert air is first solved under the same projectile velocity, gas temperature, and gas pressure as the stoichiometric hydrogen–air gas mixture. At the beginning of the reacting flow computation, the converged flowfield of the inert air is used behind the bow shock wave, but the air in front of the bow shock is replaced by a combustible gas mixture. The exothermic reaction gradually starts in the combustible gas flows through the bow shock wave.

Computational Study for Validation

The experimental conditions and the computed first Damköhler number D_I proposed in the present study are listed in Table 1. The frequency f, the period t, the period normalized by the induction time t/t_{ind}, and the frequency mode categorized into two modes, hf (high-frequency mode) and lf (low-frequency mode), are also listed in Table 1. The induction time t_{ind} is derived by the zero-dimensional analysis and is defined as the time where the temperature increase per unit time indicates a maximum value, $(\mathrm{d}T/\mathrm{d}t)_{\max}$. As shown in Table 1, the unique unsteady mode appears under the same gas condition even though the projectile velocity is varied, and the value of D_I is almost constant under the same gas condition. Furthermore, Lehr's experiment[3] reports that the instability of the reaction front disappears at the higher projectile velocity ($V = 2605$ m/s).

Although the global flowfield around the spherical projectile is important to classify unsteady features, the histories of the response of the physical variables on the stagnation streamline to the disturbance induced by the explosive gas dynamics tells us the sensitive frequency modes and strength of the perturbations. Figure 2 is such a history. Figure 3 is an x–t diagram of the density for a specific case to be discussed subsequently. Figures 2 and 4–7 show the histories of the shock standoff distance, the location of the reaction front, and the shock strength of the bow shock on the stagnation streamline. The line with open circles is the history of the shock standoff distance, and the line with closed triangles is the history of the location of the reaction front. The symbols are plotted at every 4000 iteration steps, and the time resolution is considered to be sufficient. The locations of the shock standoff distance and the reaction front are defined by the distance from the stagnation point, and the distances are normalized by the projectile radius. The shock strength, which is represented by the pressure level immediately behind the bow shock wave, is normalized by the steady shock strength. The steady shock strength is calculated by the normal shock relation with real gas effects. The frequency f and the period t roughly estimated from Figs. 2 and 4–7 and the normalized period t/t_{ind} are listed in Tables 2 and 3. Using the normalized period of the histories on the stagnation streamline, the frequency modes are categorized into three modes, hf ($t/t_{\text{ind}} \approx 1.0$), lf ($t/t_{\text{ind}} > 3.0$) and steady state (ss). The figures corresponding to the cases are listed in Tables 2 and 3.

To clarify the chemical and fluid length scale, the ratio of the induction length l_{ind} to the shock standoff distance of the sphere is also listed in Tables 2 and 3. The fluid length scale is roughly

Table 1 Experimental conditions of Lehr[3] and Ruegg and Dorsey[2]

Case	Experiment	Velocity, m/s	Pressure, atm	Diameter, mm	D_I	f, MHz	t, μs	t/t_{ind}	Mode
a	Lehr[3]	1685.0	0.421	15.0	77.64	0.148	6.76	0.763	hf
b	Lehr[3]	1931.0	0.421	15.0	77.42	0.712	1.40	1.267	hf
c	Ruegg and Dorsey[2]	1758.6	0.500	20.0	128.06	——	——	——	lf
d	Ruegg and Dorsey[2]	1963.2	0.500	20.0	127.82	——	——	——	lf

Table 2 Computational conditions for study of diameter effect

Case	Velocity, m/s	Pressure, atm	Diameter, mm	D_I	f, MHz	t, μs	t/t_{ind}	ℓ_{ind}/SSD, % (SSD = 0.16R)[a]	Mode	Figure
a-1	1685.0	0.421	5.0	25.88	——	——	——	754.25	ss	——
a-2	1685.0	0.421	10.0	51.76	——	——	——	377.13	ss	——
a-3 Exp.[3]	1685.0	0.421	15.0	77.64	0.160	6.25	0.706	251.42	hf	2a
a-4	1685.0	0.421	16.0	82.82	0.160	6.25	0.706	235.70	hf	——
a-5	1685.0	0.421	18.0	93.17	0.153	6.52	0.736	209.51	hf	2b
a-6	1685.0	0.421	20.0	103.52	0.030	33.33	3.763	188.56	lf	2c
a-7	1685.0	0.421	25.0	129.41	0.025	40.00	4.515	150.85	lf	2d
b-1	1931.0	0.421	5.0	25.81	——	——	——	100.00	ss	——
b-2	1931.0	0.421	10.0	51.61	0.750	1.33	1.203	50.00	hf	——
b-3 Exp.[3]	1931.0	0.421	15.0	77.42	0.714	1.40	1.264	33.33	hf	4a
b-4	1931.0	0.421	16.0	82.58	0.125	8.00	7.221	31.25	lf	4b
b-5	1931.0	0.421	17.0	87.74	0.143	7.00	6.318	29.41	lf	——
b-6	1931.0	0.421	18.0	92.90	0.188	5.33	4.814	27.78	lf	——
b-7	1931.0	0.421	20.0	103.22	0.143	7.00	6.318	25.00	lf	——
c-1	1758.7	0.500	5.0	32.02	——	——	——	285.50	ss	——
c-2	1758.7	0.500	10.0	64.03	0.320	3.13	0.953	142.75	hf	5a
c-3	1758.7	0.500	15.0	96.05	0.067	15.00	4.575	95.17	lf	5b
c-4 Exp.[2]	1758.7	0.500	20.0	128.06	0.053	19.00	5.795	71.38	lf	5c
d-1	1963.2	0.500	5.0	31.96	——	——	——	73.50	ss	——
d-2	1963.2	0.500	10.0	63.91	1.067	0.94	1.164	36.75	hf	6a
d-3	1963.2	0.500	15.0	95.87	0.200	5.00	6.209	24.50	lf	6b
d-4 Exp.[2]	1963.2	0.500	20.0	127.82	0.182	5.50	6.830	18.38	lf	6c

[a]SSD, shock standoff distance; R, projectile radius.

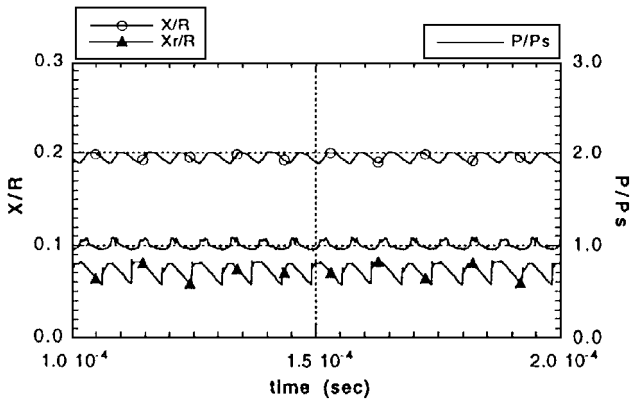

a) 15.0 mm

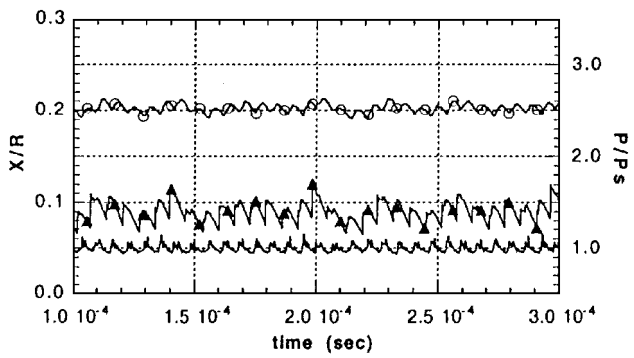

b) 18.0 mm

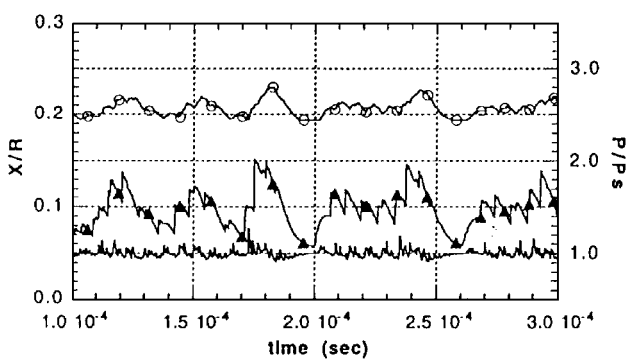

c) 20.0 mm

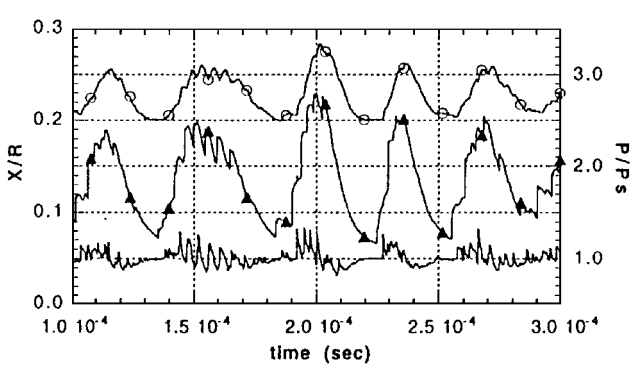

d) 25.0 mm

Fig. 2 Histories of shock standoff distance (○), location of the reaction front (▲), and shock front pressure on the stagnation streamline in the cases a-3, a-5, a-6, and a-7 in Table 2 (projectile velocity 1685.0 m/s, pressure 0.421 atm) with various diameters.

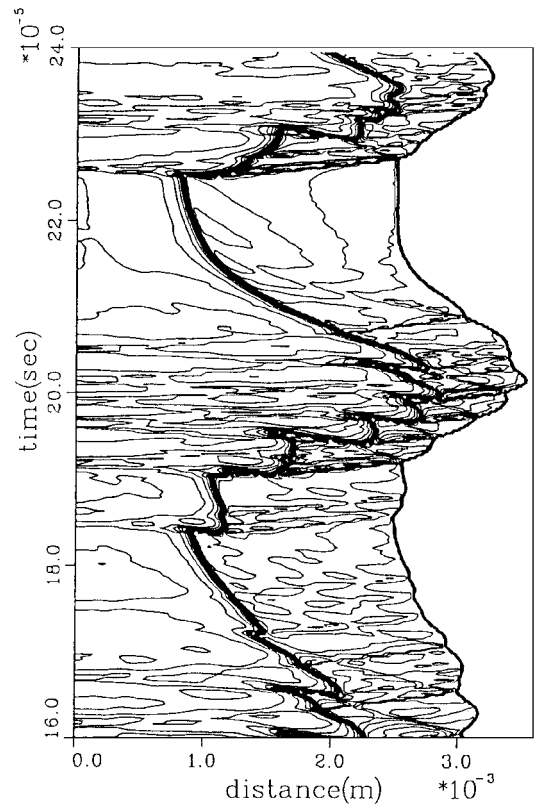

Fig. 3 Density distribution x–t diagram on the stagnation streamline in case a-7 in Table 2; projectile velocity 1685.0 m/s, pressure 0.421 atm, diameter 25.0 mm, contour range minimum = 0.7, maximum = 2.38, increase = 0.08 kg/m^3.

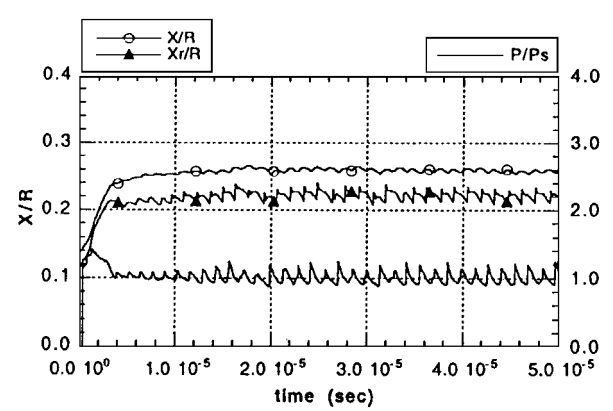

a) 15.0 mm

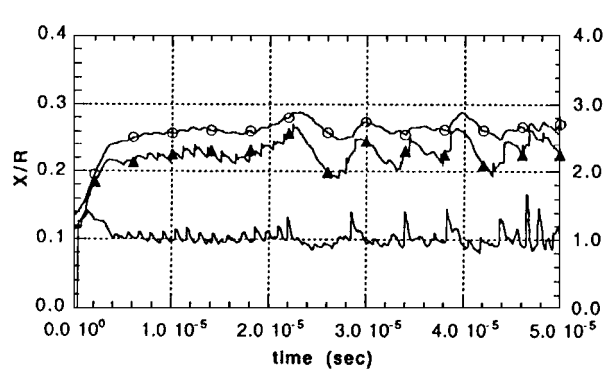

b) 16.0 mm

Fig. 4 Histories of the shock standoff distane (○), location of the reaction front (▲), and shock front pressure on the stagnation streamline in cases b-3 and b-4 in Table 2 (projectile velocity 1931.0 m/s, pressure 0.421 atm) with various diameters.

Table 3 Computational conditions for study of velocity effect

Case	Velocity, m/s	Pressure, atm	Diameter, mm	D_I	f, MHz	t, μs	t/t_{ind}	ℓ_{ind}/SSD, % (SSD = 0.16R)[a]	Mode	Figure
d-1 Exp.[2]	1963.2	0.5	20	127.82	0.182	5.50	6.830	18.4	lf	6c
c-2 Exp.[2]	1758.7	0.5	20	128.06	0.053	19.00	5.795	71.4	lf	5c
e-1	1700.0	0.5	20	127.62	0.035	28.50	4.093	149.5	lf	7a
e-2	1680.0	0.5	20	127.44	0.022	45.00	4.261	225.6	lf	7b
e-3	1650.0	0.5	20	127.15	——	——	——	877.3	ss	——

[a]SSD, shock standoff distance; R, projectile radius.

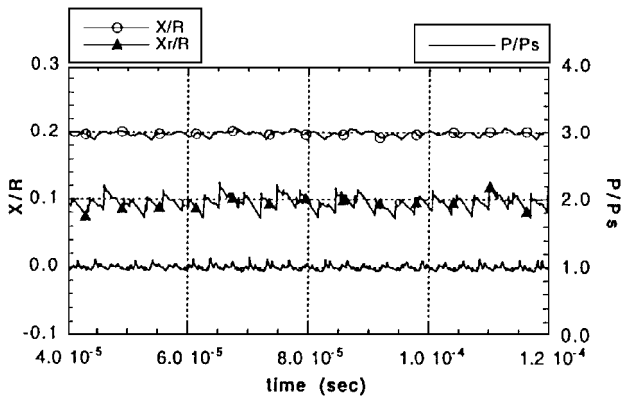

a) 10.0 mm

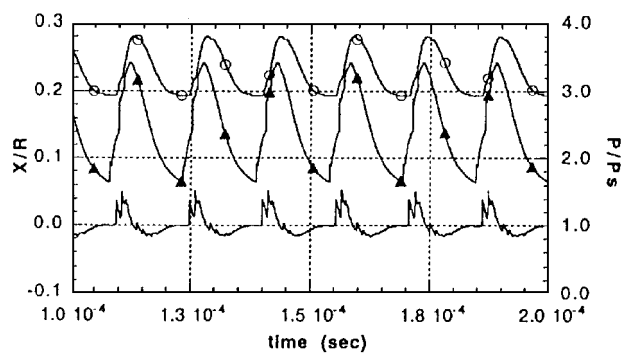

b) 15.0 mm

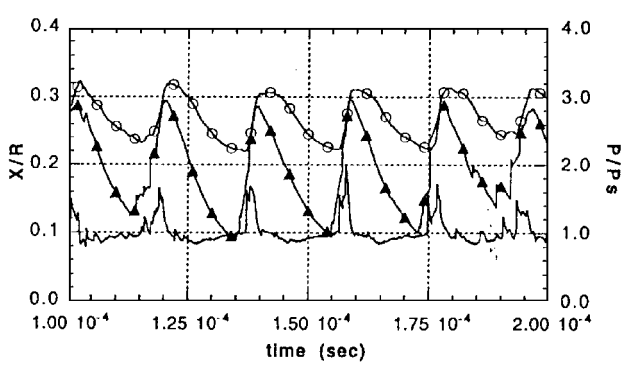

c) 20.0 mm

Fig. 5 Histories of shock standoff distance (○), location of the reaction front (▲), and shock front pressure on the stagnation streamline in cases c-1, c-2, and c-3 in Table 2 (projectile velocity 1758.7 m/s, pressure 0.5 atm) with various diameters.

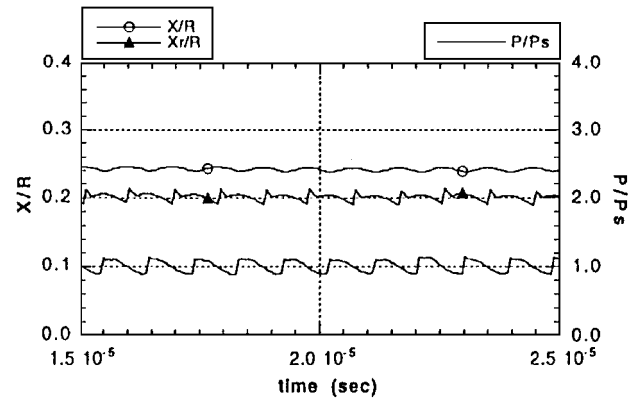

a) 10.0 mm

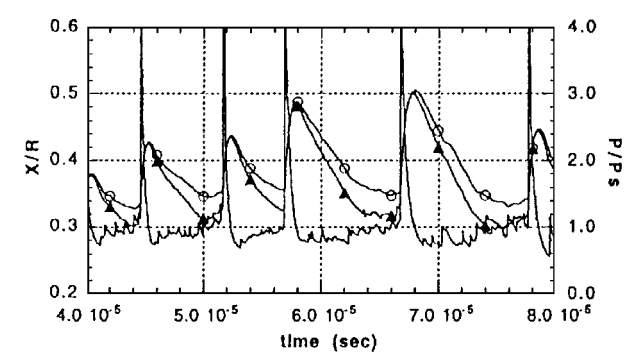

b) 15.0 mm

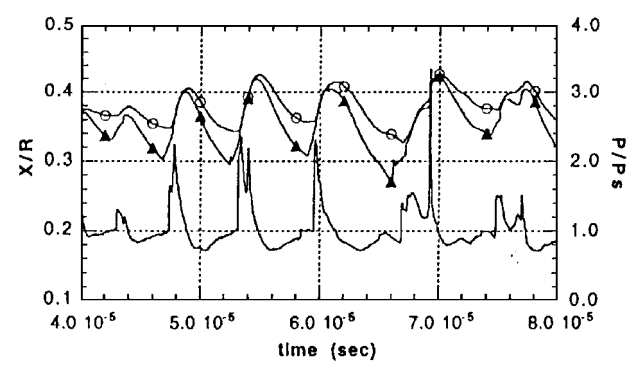

c) 20.0 mm

Fig. 6 Histories of shock standoff distance (○), location of the reaction front (▲), and shock front pressure on the stagnation streamline in cases d-1, d-2, and d-3 in Table 2 (projectile velocity 1963.2 m/s, pressure 0.5 atm) with various diameters.

estimated as 16% of the projectile radius, and the chemical length scale is obtained by the velocity behind the normal shock and the induction time derived by the zero-dimensional analysis.

Effect of Projectile Diameters

First, a series of simulations is conducted by changing the projectile diameters of cases a–d. Because D_I is a linear function of the projectile diameter [see Eq. (3)], the evaluation can be carried out straightforwardly. The corresponding computed conditions are listed in Table 2. The test gas conditions of cases a-3, b-3, c-4, and d-4 are the same as the experimental conditions of Lehr[3] and Ruegg and Dorsey[2] listed in Table 1. The induction time is indicated in Table 1 and is uniquely determined by the projectile velocity, even though the diameter is changed. The frequency mode in Table 2 is categorized by the histories on the stagnation streamline instead of the flowfield pattern around the projectile body.

Case a

Case a shows the results of various diameters in Lehr's experimental condition listed in Table 1. In cases a-1 and a-2, the solutions converged to ss although the reaction region is observed around the projectile surface. Although not shown here, the normalized

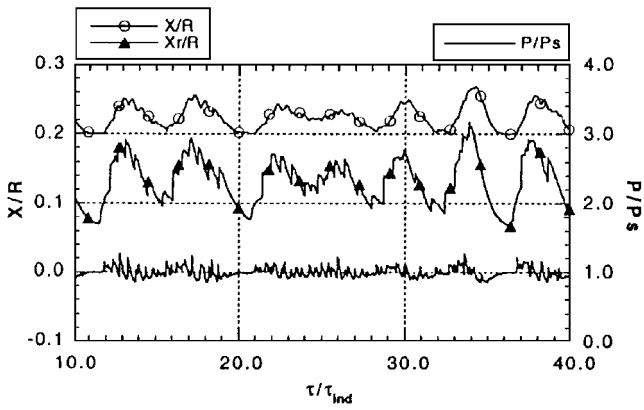

a) 1700.0 m/s

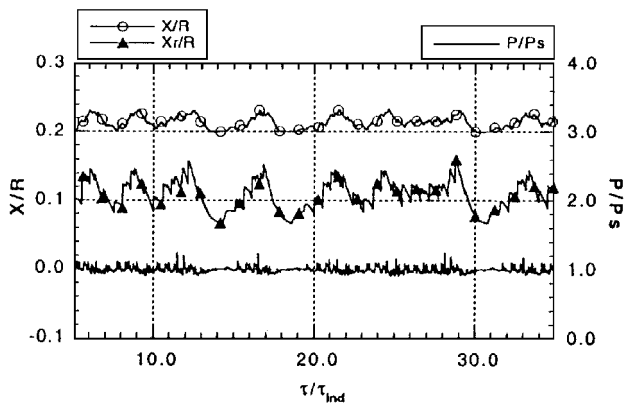

b) 1680.0 m/s

Fig. 7 Histories of shock standoff distance (○), location of the reaction front (▲), and shock front pressure on the stagnation streamline in cases e-1 and e-2 in Table 3 (diameter 20.0 mm, pressure 0.5 atm) with projectile velocity.

shock pressure histories settle to be constant 1.0, which indicates no oscillation occurs behind the bow shock. This mode is categorized into ss, which is a converged steady solution. Cases a-3–a-7 show unsteady behaviors on the stagnation streamline, as shown in Figs. 2a–2d. Case a-3 is Lehr's experimental condition, and the histories on the stagnation streamline are shown in Fig. 2a. According to the experiment,[1] the high-frequency mode (0.148 MHz) of the regular regime is observed. The unsteady feature of the simulation result in case a-3 shows the high-frequency mode (0.160 MHz) in the history (Fig. 2a) and the regular regime of the flowfield. It can be said that the experimental flow feature is reproduced by the simulation result. Case a-4 also shows regularly repeated high-frequency oscillations. In case a-5, high-frequency oscillations are also observed, but the range of the amplitude of the reaction front location is not completely constant, as shown in Fig. 2b. Figure 2c shows case a-6. The low-frequency oscillations clearly appear in the high-frequency mode. The amplitude of the reaction front in Fig. 2c is much higher than those in Figs. 2a and 2b, but the reaction front is always away from the location of the bow shock wave. Therefore, the pattern of the flowfield in case a-6 can be categorized into the regular regime, although the histories on the stagnation streamline are categorized into the low-frequency mode. This result indicates the presence of the exceptional case in which the regular regime flow pattern in the flowfield shows the low-frequency oscillation on the stagnation streamline. In Fig. 2d (case a-7), the low-frequency oscillation is clearly observed in the shock standoff distance, as well as the reaction front. However, the history of the shock pressure does not have a strong peak in a cycle and still shows the summation of high-frequency oscillations. The reaction front in Fig. 2d is always away from the bow shock, as was the case in Fig. 2c. The x–t diagram of the density history on the stagnation streamline is shown for case a-7 in Fig. 3. The reaction front moves rightward and leftward with the low-frequency mode but never penetrates the bow shock. That is the reason a strong peak in one cycle does not appear in the shock pressure history in Fig. 2d. On the other hand, the reaction front is strengthened by the self-enforced explosions,[15] in which new reactions are intermittently created in one cycle.

Case b

Case b shows the result of the various diameters in the Lehr experimental condition listed in Table 1. According to the experiment, the high-frequency mode (0.712 MHz) of the regular regime of the unsteady shock-induced combustion is observed. In case b-1 with the diameter 5.0 mm, the steady solution is obtained. Case b-2 shows the regularly repeated high-frequency mode. The histories of case b-3, in Fig. 4a, which correspond to Lehr's experimental condition in Table 1, show the high-frequency mode, and the frequency in the simulation result (0.714 MHz) agrees well with the experimental data. In cases b-4–b-7, the low-frequency mode appears in the histories and is dominant in the oscillation modes. The histories of case b-4 are shown in Fig. 4b, which shows the transition from the high-frequency mode to the low-frequency mode. The high-frequency oscillations are observed until 20.0 μs, when the low-frequency mode appears. Then the histories and the flowfield are completely changed. After the initiation of the low-frequency mode, the density contour plots show the typical features of the large-disturbance regime.

Case c

Cases c and d are the experimental conditions of Ruegg and Dorsey.[2] Both the experimental and computational results in the past showed the large-disturbance regime of the unsteady combustion.[15]

As shown in Table 2, case c-1, in which the projectile diameter is 5.0 mm, shows the converged ss solution, similar to cases a-1, a-2, and b-1. In Fig. 5a, which is case c-2, the high-frequency mode appears in all of the histories and is dominant. As shown in Fig. 5b, all of the histories for case c-3 are regularly repeated, and the low-frequency mode is dominant. The condition of case c-4 in Table 2 is the same as the experimental conditions of case c in Table 1. The experiment shows the typical large-disturbance regime of the unsteady combustion. In Fig. 5c (case c-4), all of the histories indicate periodic and high amplitude oscillations. The pressure peak level is more than 1.5 times the steady pressure level. As discussed in previous works,[15] the flowfield around the projectile shows the typical shock-reaction front interaction pattern of the large-disturbance regime.

Case d

Case d is the experimental conditions of Ruegg and Dorsey,[2] and the large-disturbance regime appeared in both the experiment and the computation.[15] As shown in Table 2, case d-1, in which the projectile diameter is 5.0 mm, shows the converged ss solution. In case d-2, the histories show the high-frequency mode, as shown in Fig. 6a, and the flowfield is a typical regular regime of shock-induced combustion. Figures 6b and 6c show cases d-3 and d-4, and these histories have a strong peak in one cycle. These cases show the typical large-disturbance regime of unsteady shock-induced combustion.

Summary of Diameter Effect

The effect of the diameters was clarified by a series of computations. The computed results in cases a–d show that the unsteady regime changes from the regular regime to the large-disturbance regime when the projectile diameter is increased. The results in case b suggest that the first Damköhler number 80.0 is a critical value for the unsteady regime of shock-induced combustion around the spherical projectile. For cases c and d, the unsteady regime clearly changes across the first Damköhler number 80.0. According to the study, the proposed first Damköhler parameter works well and can categorize the unsteady flow regime.

Effect of Projectile Velocity

In the preceding section, the effect of the diameters was investigated by a series of simulations. According to the proposed first Damköhler parameter, the projectile velocity shows little effect on the change of the first Damköhler value (see Table 2). However,

the unsteady mode is very sensitive to the diameter and the test gas pressure. In this section, the effect of the projectile velocity is investigated using the test gas condition of Ruegg and Dorsey[2] (Table 1) in which the low-frequency mode (large-disturbance regime) is observed. Slower velocities are chosen than in the Ref. 2 experiments, as listed in Table 3. The histories of the shock standoff distance, the location of the reaction front, and the bow shock strength on the stagnation streamline are also used in this study for velocity effect. The time in Figs. 7 is normalized by the induction time of each case inasmuch as the induction time is varied by the shock strength.

In the histories shown in Figs. 7, which are cases e-1 and e-2, the low-frequency mode is dominant in the plots of the shock standoff distance and the location of the reaction front, but the histories of the shock pressure have several peaks in one cycle of the low-frequency oscillations. The features are similar to those in Figs. 2c and 2d. In case e-3, the computed result converges to the steady solution though the reaction occurs in a thin region around the projectile surface. The induction time is exponentially related to the projectile velocity. In comparing case e-2 with case e-3, the induction length in case e-3 is about four times longer than that in case e-2, even though the velocity change is only less than 2%. To discuss the unsteadiness of shock-induced combustion, the effect of the induction time and the length must be taken into account.

The results suggest that the projectile velocity is not the key factor to determine the unsteady mode because a unique unsteady mode appears in the same gas condition, such as pressure, temperature, and the gas mixture under the fixed projectile diameter, and in the range of the lower and higher velocity, the unsteadiness disappears and converges to the steady solution. Therefore, the idea of the proposed first Damköhler parameter is that the unsteady mode is potentially given by the test conditions.

Applicable Range of Prediction Method

The proposed first Damköhler parameter is regarded as the strength of the reaction shock. The parameter value 80.0 must be the critical shock strength to induce the low-frequency mode. When the projectile velocity is slower, the gas temperature behind the bow shock is lower. Because the induction time is an exponential function of the gas temperature, the lower gas temperature makes the induction time and length longer. Supposing that the strength of the reaction shock is constant, the lower projectile velocity case would require several explosions or reaction shocks in one cycle to induce the low-frequency mode, so-called self-enforced explosions,[15] as shown in Fig. 3.

Cases a-4 ($D_I = 82.82$) and a-5 ($D_I = 93.17$) do not show the low-frequency mode in the simulation results. As observed in Figs. 2 and 3, all of the results in case a do not show the typical features of the large-disturbance regime, such as the penetration of the reaction front and the onset of the detonation wave. In a sense, the strength of reaction shock is considered to be weaker. Actually, the projectile velocity of case a is lower than that of cases b–d, and in cases a-4 and a-5 the induction length derived analytically is more than two times the shock standoff distance. Therefore, a series of reaction shocks is required in one cycle to induce the low-frequency mode. Normally, the averaged period of the large-disturbance regime is about 5.23 times the induction time and is about 5 times longer than that of the regular regime. Even in case a-3, the period is so long that one corrugated pattern on the reaction boundary is seen only in the computed domain in the present study. It is supposed that the wave interaction of the low-frequency mode cannot be initiated by reaction shocks because the summation of wave propagating times in one cycle is too long to form the self-enforced explosions. Observing Fig. 2b, the high-frequency oscillations of shock and reaction front locations are not completely constant, but the low-frequency mode is not dominant for the reasons given earlier. It can be said that, in the case of $D_I \leq 94$, the induction length should be less than 200% of the shock standoff distance to induce the low-frequency mode in the flowfield. In case e-2, the low-frequency mode appears in the flowfield though the induction length is more than 200% of the shock standoff distance. The reason is that the parameter value is $D_I = 127.44$, and the strength of the reaction shock is much stronger than in cases a-4 and a-5.

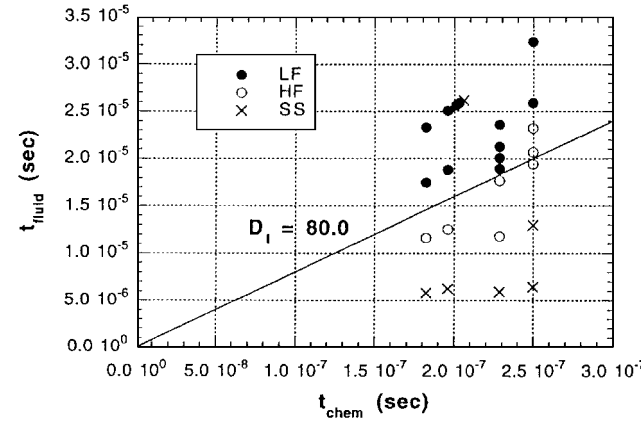

Fig. 8 Chemical and fluid characteristic timescales derived by the prediction method. Modes (lf, hf, and ss) are obtained by the experiments or the simulation results. Critical first Damköhler number distinguishing the high-frequency mode from the low-frequency mode is 80.0.

Under an arbitrary condition, such as the proposed first Damköhler parameter, the ratio of the induction length to the shock standoff distance is easily calculated by zero-dimensional analysis. Some cases have to take into account the applicable range of the prediction method. The variables for such consideration are all derived from the zero-dimensional analysis, and then the expected unsteady mode is easily estimated.

Summary of Validation

The simulation results in Tables 2 and 3 are categorized into three modes, ss, hf, and lf. The chemical and fluid characteristic times are derived from the prediction method, and the location of each plot is determined only by the zero-dimensional analysis without simulations. They are plotted in Fig. 8. The symbols ●, ○, and × show each unsteady mode that appears in the simulations. The inclination of the linear line in Fig. 8 indicates the first Damköhler number D_I. The number indicates that the criterion of the unsteady mode between the low-frequency mode and high-frequency mode. The high-frequency mode, mainly corresponding to the regular regime, occurs in the region below the line for $D_I = 80.0$, and the low-frequency mode, mainly corresponding to the large-disturbance regime, occurs in the region above that line. The present method can predict the two distinct unsteady modes, which are potentially determined by the test gas conditions and the projectile diameter without an additional disturbance, by the numerical technique and experimental operation. However, the actual experiments cannot get rid of initial disturbances by the operation, and the disturbances strongly depend on the apparatus itself. Therefore, the limitation of the prediction method exists when the prediction method is used for the estimation of the experimental condition.

Conclusions

An effective nondimensional parameter, referred to as the first Damköhler number, is proposed for the prediction of the unsteady flow regime in shock-induced combustion around a hypervelocity spherical projectile into a stoichiometric hydrogen–air gas mixture. The parameter consists of the ratio of the fluid characteristic timescale to the chemical characteristic timescale. The fluid characteristic time was defined as a projectile diameter over a speed of sound, and the chemical characteristic time was defined as a temperature over the maximum value of a temperature increase for the exothermicity per unit time. The conditions of the speed of sound and the temperature were assumed to be immediately behind the bow shock in front of the spherical projectile and were obtained by the normal shock relations under real-gas effects. The temperature increase for the exothermicity was estimated by time integration of the species equations in zero dimension in space under the constant-volume mode. The first Damköhler number defined here works well for the prediction of unsteady shock-induced combustion around spherical projectiles and quantitatively distinguishes two distinct flow regimes observed in experimental and numerical results under

arbitrary conditions. The first Damköhler number is obtained by a small analytical computation estimating the chemical and fluid characteristics without time-consuming unsteady flow simulations or experimental facilities. Also, the applicable range of the prediction method is discussed, based on the mechanism of the unsteady shock-induced combustion.

References

[1]Alpert, R. L., and Toong, T. Y., "Periodicity in Exothermic Hypersonic Flow About Blunt Projectiles," *Astronautica Acta*, Vol. 17, Nos. 4, 5, 1972, pp. 539–560.

[2]Ruegg, F. W., and Dorsey, W., "A Missile Technique for the Study of Detonation Waves," *Journal of Research of the National Bureau of Standards*, Vol. 66C, No. 1, 1962, pp. 51–58.

[3]Lehr, H. F., "Experiments on Shock-Induced Combustion," *Astronautica Acta*, Vol. 17, Nos. 4, 5, 1972, pp. 589–597.

[4]McVey, J. B., and Toong, T. Y., "Mechanism of Instabilities of Exothermic Hypersonic Blunt-Body Flow," *Combustion Science and Technology*, Vol. 3, No. 2, 1971, pp. 63–76.

[5]Chernyi, G. G., "Supersonic Flow Past Bodies with Formation of Detonation and Combustion Fronts," *Astronautica Acta*, Vol. 13, Nos. 5, 6, 1968, pp. 467–480.

[6]Behrens, H., Struth, W., and Wecken, F., "Studies of Hypervelocity Firings into Mixtures of Hydrogen with Air or with Oxygen," *Tenth Symposium (International) on Combustion*, Combustion Inst., Pittsburgh, PA, 1965, pp. 245–252.

[7]Matsuo, A., and Fujiwara, T., "Numerical Investigation of Oscillatory Instability Mechanism in Shock-Induced Combustion Around an Axisymmetric Blunt Body," *AIAA Journal*, Vol. 31, No. 10, 1993, pp. 1835–1841.

[8]Matsuo, A., Fujii, K., and Fujiwara, T., "Flow Features of Shock-Induced Combustion Around Projectile Traveling at Hypervelocities," *AIAA Journal*, Vol. 33, No. 6, 1995, pp. 1056–1063.

[9]Wilson, G. J., and Sussman, M. A., "Computation of Unsteady Shock-Induced Combustion Using Logarithmic Species Conservation Equations," *AIAA Journal*, Vol. 31, No. 10, 1993, pp. 294–301.

[10]Wilson, G. J., "Computation of Steady and Unsteady Shock-Induced Combustion over Hypervelocity Blunt Bodies," Ph.D. Thesis, Dept. of Aeronautics and Astronautics, Stanford Univ., Stanford, CA, Dec. 1991.

[11]Sussman, M. A., "Numerical Simulation of Shock Induced Combustion," Ph.D. Thesis, Dept. of Aeronautics and Astronautics, Stanford Univ., Stanford, CA, Dec. 1994.

[12]Ahuja, J. K., Tiwari, S. N., and Singh, D. J., "Investigation of Hypersonic Shock-Induced Combustion in Hydrogen-Air System," AIAA Paper 92-0339, Jan. 1992.

[13]Ahuja, J. K., and Tiwari, S. N., "Numerical Simulation of Shock-Induced Combustion in a Superdetonative Hydrogen–Air System," AIAA Paper 93-0242, Jan. 1993.

[14]Matsuo, A., and Fujii, K., "Computational Study of Large-Disturbance Oscillations in Unsteady Supersonic Combustion Around Projectiles," *AIAA Journal*, Vol. 33, No. 10, 1995, pp. 1828–1835.

[15]Matsuo, A., and Fujii, K., "Detailed Mechanism of the Unsteady Combustion Around Hypersonic Projectiles," *AIAA Journal*, Vol. 34, No. 10, 1996, pp. 2082–2089.

[16]Ahuja, J. K., and Tiwari, S. N., "Effect of Various Flow and Physical Parameters on Stability of Shock-Induced Combustion," AIAA Paper 96-0732, Jan. 1996.

[17]Abouseif, G. E., and Toong, T. Y., "Theory of Unstable One-Dimensional Detonations," *Combustion and Flame*, Vol. 45, 1982, pp. 67–94.

[18]Fickett, W., and Wood, W. W., "Flow Calculations for Pulsating One-Dimensional Detonations," *Physics of Fluids*, Vol. 9, No. 5, 1966, pp. 903–916.

K. Kailasanath
Associate Editor